White Matter Hyperintensities in the Forties: Their Prevalence and Topography in an Epidemiological Sample Aged 44–48

Wei Wen,[1,2]* Perminder S. Sachdev,[1,2] Jason J. Li,[3] Xiaohua Chen,[1,2] and Kaarin J. Anstey[4]

[1]*Neuropsychiatric Institute, Prince of Wales Hospital, Randwick, New South Wales, Australia*
[2]*School of Psychiatry, University of New South Wales, Sydney, Australia*
[3]*School of Computer Science and Engineering, University of New South Wales, Sydney, Australia*
[4]*Centre for Mental Health Research, Australian National University, Canberra, Australia*

Abstract: White matter hyperintensities (WMHs) are a frequent finding on T2-weighted MRI of the brain in elderly individuals, but their prevalence and severity in younger asymptomatic populations is less well studied. We report the topography of WMHs on T2-weighted fluid inversion recovery (FLAIR) MRI in 428 individuals aged 44-48 years recruited randomly from a healthy community sample. WMHs were delineated from FLAIR and T1-weighted scans by using a computer algorithm, further verified and then classified using *k*-nearest neighbor (kNN) algorithm into deep WMH (DWMH), and periventricular WMH (PVWMH), which included extended periventricular "rims" and frontal and occipital "caps". Small caps and pencil-thin rims were not taken as WMHs for this analysis. The new computer algorithm was validated and compared with the scores of visual rating, and the correspondence between the two methods was high. We found that 218 (50.9%) subjects had WMHs. 146 of the 218 (34.1% of whole sample population of 428) subjects had deep white matter hyperintensities (DWMHs). The average number of WMH clusters (occurrences) per brain was 1.37 (0.94 for DWMH and 0.43 for pathological PVWMH) and the mean WMH tissue volume was 0.278 ml. There was no significant sex difference in the severity and distribution of WMHs. The study suggests that small punctate or focal WMHs are common in the brains of individuals in their 40s, and may represent an early stage of development of these lesions. *Hum Brain Mapp 30:1155–1167, 2009.*

Key words: white matter hyperintensity; MRI; automated detection; topography; prevalence

INTRODUCTION

White matter signal changes in the brain MRI scans, most conspicuously seen as foci of high signal intensity in T2-weighted scans, are often found in the brains of asymptomatic elderly individuals as well as in disease-specific brains [Fazekas, 1989; Fazekas et al., 1993; Ylikoski et al., 1995; Wen and Sachdev, 2004a,b]. In asymptomatic populations, the prevalence of white matter hyperintensities (WMHs) increases pointedly with increasing age [Enzinger et al., 2006; Fazekas, 1989; Schmidt et al., 2002].

Normal brain white matter contains nerve fibers, neuroglial cells, vascular structures, and interstitial space. The nerve structures in the white matter are mainly axons, surrounded by a myelin sheath, while the nerve cell bodies are located in the cerebral cortex. Damage to the white matter can be seen as a range of changes, which include demyelination, destruction of axons, change in glial cell numbers, and finally cavitation and infarction. The relaxa-

Contract grant sponsor: National Health and Medical Research Council (NHMRC) of Australia; Contract grant numbers: 157125 and 179805.

*Correspondence to: Wei Wen. E-mail: w.wen@unsw.edu.au

Received for publication 2 July 2007; Revised 15 January 2008; Accepted 6 March 2008

DOI: 10.1002/hbm.20586

Published online 8 May 2008 in Wiley InterScience (www.interscience.wiley.com).

tion times of the tissue in MRI are regulated by its physical, chemical, and biological properties. In regions of white matter pathology, therefore, the high water content and the degeneration of macromolecular structure leads to alteration in the tissue's relaxation rates. As a result, it is seen as a higher intensity signal on T2-weighted scans such as the fluid attenuated inversion recovery (FLAIR) sequence MRI, the so-called WMHs or leukoaraiosis. T2-weighted MRI is particularly sensitive in detecting these abnormalities, but the appearance is not specific to any etiology.

WMHs have been found to be associated with altered apparent diffusion coefficient (ADC) values [Helenius et al., 2002]. ADC, obtained by diffusion weighted MRI (DWI) [Le Bihan, 1991], represents rate of water diffusion in a particular region and can be used to evaluate microstructural integrity [Mascalchi et al., 2002a,b]. Postmortem examination confirms that WMHs are correlated with histopathologic changes [Fazekas et al., 1993; Scheltens et al., 1995; Smith et al., 2000; Takao et al., 1999]. White matter abnormalities, such as punctate, early confluent, and confluent WMHs, corresponded to increasing severity of ischemic tissue damage, ranging from mild perivascular alterations to large areas with variable loss of fibers, multiple small cavitations, and marked arteriolosclerosis. Microcystic infarcts and patchy rarefaction of myelin are also characteristics of irregular periventricular high signal intensities. There is a strong relationship between the extent of WMHs on MRI and the extent of gross and microscopic changes seen in the white matter of myelin-stained sections [Smith et al., 2000]. Hyperintense periventricular caps lining the frontal and occipital horns, and a smooth halo bordering the walls of the lateral ventricles, on the other hand, may be nonischemic in origin and comprise areas of demyelination associated with subependymal gliosis associated with discontinuity of the ependymal lining [Fazekas et al., 1993]. These have been referred to as periventricular WMHs (PVWMHs), which not infrequently extend into the deep white matter.

High prevalence of WMHs among healthy elderly populations, e.g. those aged greater than 70, has been reported in many studies [Enzinger et al., 2006; Fazekas, 1989; Hopkins et al., 2006; Schmidt et al., 2003; de Leeuw et al., 2001; Wen and Sachdev, 2004b; Longstreth et al., 1996; Ylikoski et al., 1993]. In contrast to the wealth of studies focusing on the disease-specific and elderly population, relatively few studies have examined younger asymptomatic populations [Fazekas, 1989; Hopkins et al., 2006]. The reports on the younger samples have been less consistent. One earlier study [Fazekas, 1989] reported an 11% prevalence in the 4th decade of life of symptom-free subjects. In a recent study [Hopkins et al., 2006], WMHs were found in only around 6% of the subjects in the age range of 46–55. An earlier study from our group demonstrated the high prevalence of WMH in a population aged 60–64 years, i.e. those still in mid-age [Wen and Sachdev, 2004a]. The examination of WMHs in young individuals is important for a variety of reasons. If the pathogenesis of these lesions is to be understood and potentially modifiable factors to be identified, the study of individuals in the earliest stages of development of the lesions would be valuable. Moreover, the functional consequences of these lesions in mid-life are of interest as many noncognitive neuropsychiatric syndromes have been related to the lesions. We therefore asked the question: do WMHs occur in the brains of even younger healthy individuals? To answer this question effectively and accurately, there was a need for an automated method of accurate detection and classification of early WMHs, which presumably were very small in size, and could easily be missed if using visual ratings. Most of the WMH prevalence studies used visual ratings of WMHs, which generally would fail to capture the full diversity in WMH distribution and unable to describe the topography of the lesions. The aim of this work was then to explore this important question by measuring the topography of the WMHs in the brains of a large healthy sample drawn from a community-dwelling population aged 44–48 by developing an automated method for WMH measurement.

Along with manual delineation and human-supervised semi-automated segmentation, such as local thresholding [Rovaris et al., 1997] and seed growing, automated methods of WMH segmentation have been increasingly explored and implemented, e.g. k-nearest neighbor (kNN) classification rule [Duda et al., 2001] was used to automatically label the brain image voxels into grey matter, white matter, CSF, and WMH voxels [Anbeek et al., 2004; Wu et al., 2006]. These methods were mainly used for detecting relatively large or confluent WMH clusters such as those normally found in multiple sclerosis patients [Wu et al. 2006] or elderly subjects. One of the technical challenges in this work was the design and implementation of the computer algorithms for automatic identification and classification of WMHs due to the fact that WMHs in this age group appeared to be sparse and focal. A small error resulted from the algorithm in absolute value, either in the number of WMH occurrences or the volume of WMH clusters, would lead to perhaps unacceptable and misleading results. A new algorithm, both sensitive and robust to the focal and sparse lesions, based on kNN rule application on the WMH clusters validation was developed for this study. The method is fully described in this paper along with the WMH topographic findings.

Many studies have separated WMHs into two broad categories: periventricular (PVWMH) and deep (DWMH), depending on the proximity of these WMHs to the lateral ventricles. This distinction has been supported by results of some studies, e.g., an increase in PVWMH, but not DWMH, was in parallel with cognitive decline in nondemented subjects [van den Heuvel et al., 2006], and some other studies suggested that DWMH were more strongly correlated with vascular risk factors [Fazekas et al., 1987; Wen and Sachdev, 2004b]. While it is clear that certain locations are more relevant than others depending on the type of function probed, the separation of WMH purely on

TABLE I. Descriptive characteristics of the subjects included in the study

	Total (N = 428)	Male (N = 196)	Female (N = 232)	Comparison between male and female		
				df	t/χ^2	P value
Age in years[a]	46.69 (1.43)	46.64 (1.50)	46.73 (1.37)	426	−0.649	0.517
Education in years[a]	14.80 (2.27)	15.02 (2.22)	14.61 (2.30)	425	1.869	0.062
Right-handed[b]	381 (89.0)	174 (88.8)	207 (89.2)	1	0.022	0.882
Scanner A[b]	163 (38.1)	90 (45.9)	73 (31.5)	1	9.412	0.002*

P-values are for 2-tailed t-tests of continuous variables and χ^2 tests of discrete variables between male and female.
*$P < 0.05$.
[a] Mean (SD).
[b] Number of occurrences and the percentage (%).

its proximity to the ventricles has been questioned [Barkhof and Scheltens, 2006; DeCarli et al., 2005b; Sachdev and Wen, 2005] To examine and address this issue and use the data meaningfully in further studies examining the relationships between WMHs and the clinical risk factors and/or cognitive functioning, we have implemented in the algorithms the accurate measurement of the distances of WMHs to the wall of lateral ventricles for every brain.

SUBJECTS AND METHODS

Subjects

The study sample was drawn from the Personality and Total Health (PATH) Through Life project. PATH is a longitudinal study of three cohorts aged 20–24, 40–44, and 60–64 years, all comprising community residents recruited randomly through electoral rolls from the city of Canberra and the adjacent town of Queanbeyan, Australia. Enrolment to vote is compulsory for citizens of Australia. The cohorts are examined every 4 years, and this cohort was in the age range 44-48 years at the time of examination, which was Wave 2 of the study. The study included a total of 2,530 people, of which 656 were randomly offered an MRI. 503 participants accepted MRI and 431 (85.7%) eventually had an MRI scan. The reasons for not undergoing an MRI scan after having initially agreed included subsequent withdrawal of consent, medical conditions contradicting MRI, and claustrophobia or other anxiety about the procedure. There were no differences in age, sex, and years of education between those who had an MRI scan and those who did not ($P > 0.05$). Of those 431 subjects who had MRIs, the imaging data for one subject were lost because of an operational error, and another was scanned with FLAIR sequence only, making the final number of subjects with complete set of imaging data as 429. One subject was found to have a large cyst across right occipital, posterior temporal, and parietal lobes, leading to his exclusion, thereby leaving 428 subjects for final analysis. Handedness was assessed by Edinburgh Handedness Inventory [Oldfield, 1971]. The study was approved by the ethics committees of the Australian National University, Canberra and the University of New South Wales, Sydney, Australia.

Some descriptive characteristics of the sample are presented in Table I. Subjects with and without MRI scans in the entire sample did not differ on age, sex, years of education, mini-mental state examination (MMSE) scores, and the prevalence of putative risk factors for brain WMH and atrophy, indicating that there was no obvious selection bias within the study sample.

Image Acquisition

Imaging was conducted with a 1.5 T Gyroscan (ACS-NT, Philips Medical Systems, Best, Netherlands) for T1-weighted 3D structural and T2-weighted FLAIR sequence MRI. A 2D scout mid-sagittal cut for AC-PC plane alignment was first acquired (TR/TE/NEX = 500/16/1.5; slice thickness = 5 mm). Both T1-weighted 3D structural MRI and T2-weighted FLAIR images were then acquired in coronal plane. About mid-way through this study, for reasons outside the researchers' control, the original scanner (scanner A) was replaced with a similar Philips scanner (scanner B). Although there was a change of the scanner during the study, there was no significant alteration in acquisition parameters. The first 163 subjects were scanned with scanner A for T1-weighted 3D structural MRI with TR = 8.84 ms, TE = 3.55 ms, flip angle = 8°, matrix size = 256 × 256 and FOV = 256, yielding in-plane resolution of 1 × 1 mm/pixel and slice thickness = 1.5 mm with no gap between slices. The FLAIR sequence was acquired with TR = 11,000 ms, TE = 140 ms, TI = 2,600; matrix size = 256 × 256; FOV = 230 × 230 mm; slice thickness = 4.0 mm with no gap between slices, yielding in-plane spatial resolution of 0.898 × 0.898 mm/pixel. The acquisition parameters of T1-weighted 3D structural MRI for the remaining 268 subjects (431–163 = 268) on scanner B were TR = 8.93 ms, TE = 3.57 ms, flip angle 8°, matrix size and FOV remained the same as scanner one, producing the same in-plane resolution and slice thickness. There was no change of the parameters for FLAIR sequence. The total time of each subject's scanning session was approximately 20 min. To ensure the reliability and compatibility of the

data, we compared the subjects scanned on the two scanners on sociodemographic and imaging parameters. There were no differences in age ($P = 0.377$) or years of education ($P = 0.588$), but more women were inadvertently scanned on the scanner B than A ($P = 0.003$). The volumetric measures of total intracranial volume (TIV) ($P = 0.697$), gray matter (GM) volume ($P = 0.934$), white matter (WM) volume ($P = 0.165$), or cerebrospinal fluid (CSF) volume ($P = 0.820$) obtained from the two scanners did not differ.

Image Processing

MRI data were transferred to a DELL Precision 390 workstation running Windows XP®. In our previous work [Wen and Sachdev, 2004a], WMH estimation was implemented in the Talairach space, i.e. co-registered FLAIR and T1 scans of the same subject were spatially normalized into Talairach space, and the classification and volumetric estimation of WMH distribution were then performed in this "standard space". After visual inspection of the FLAIR scans of this age group, we decided to modify our computational approach for two reasons: (a) although WMHs, including DWMH and PVWMH, were observed in some of the subjects' FLAIR scans, these WMHs, especially DWMH, appeared to be both focal and sparse, and were difficult to detect because of their reduced intensity and increased fuzziness if mapped into Talairach space; (b) given the nonlinearity of the mapping, the WMHs thus classified were no longer the absolute volumes. Therefore, the automatic classification of WMHs employed in this study was carried out in the original acquisition space of the T1-weighted structural images. Five preprocessing steps were taken to prepare the images for the WMH classification and analysis. These are as follows: (1) as the information for WMH classification was from both FLAIR and T1-weighted MRI scans, we co-registered the FLAIR and 3D T1 structural images of the same subject using mutual information method [Wells et al., 1996], with T1 as target and FLAIR as source; (2) segmentation [Ashburner and Friston, 1997, 2005] of T1-weigthed structural images into three separate tissue components, i.e. GM, WM, and CSF; (3) removal of nonbrain tissue from both T1-weighted and co-registered FLAIR images using the brain mask transformed from the average mask originally defined in the Talairach space by inverting the deformation matrix generated from its own spatial normalization [Ashburner and Friston, 1999]; (4) inverting the spatial normalization transformation to produce the brain masks and white matter probability maps in the individual imaging space for the WMH detection and non-brain tissue removal; (5) intensity correction [Ashburner and Friston, 2005] of both FLAIR and T1-weighted images after the removal of nonbrain tissues. Some other smaller steps such as removal of the bright areas observed in the FLAIR sequence ventricles caused by choroid plexus and partial voluming were also carried out. SPM2 (Wellcome Department of Cognitive Neurology, Institute of Neurology, London, UK) software package was used with Matlab 7.1 (MathWorks, Natick, MA) for these preprocessing steps.

The Calculation of Distances Between WMHs and Lateral Ventricles

To investigate how WMHs were spatially distributed in the brain, and more importantly, to be able to study the separate influence of DWMH and PVWMH on function, we defined the perpendicular distance from the centroid of a WMH cluster to the nearest edge of lateral ventricles as the distance between a WMH cluster and lateral ventricle. For the efficient calculation of the distance between each WMH cluster to lateral ventricles, we created a 3D image (distance map) of the same dimension as the scan and each voxel of the image had the distance of the voxel to the nearest edge of lateral ventricles as the intensity value. To create this 3D image, we manually traced the ventricles from the T1 image of the subject and then applied morphological dilation to the image of traced ventricles. To compensate for the elongation as a result of the original voxel dimensions, the 3D structuring matrix was rescaled accordingly. The image was then dilated with this rescaled matrix until the entire image was filled. To calibrate for the world-coordinate distance of any given voxel to the ventricles, we first identified the voxels with maximum and minimum values in the resulting image. The real world-coordinate distance was the Euclidian difference of their voxel positions multiplied by the voxel dimensions of the image. The distance map for any given voxel or the centroid of a cluster of voxels of an extracted WMH map could then be obtained with a dot multiplication of the binary WMH image and the ventricle dilation image $I_{\text{Distance}} = I_{\text{WMH}} \cdot I_{\text{VentricleDilation}}$.

Initial WMH Detection

The contrast properties of FLAIR sequence MRI facilitate the possibility of automated segmentation and classification of WMH. Although the intensities of WMH, gray matter, white matter and CSF can be listed sequentially in order of decreasing intracranial signal intensity, there is considerable overlap of signal intensities between these tissue components. A parametric method [Wen and Sachdev, 2004a] was adapted and applied to the initial WMH detection. The white matter probability map used as a weighting function in this procedure was transformed into the image acquisition space from the Talairach space by inverting the deformation matrix of spatial normalization. The purpose of this detection was to extract candidate WMH clusters from the brain. The extracted candidate WMH clusters were further investigated using a non-parametric kNN rule and then classified into DWMH (pathological), PVWMH, and the false WMH clusters. PVWMH were further classified into pathological PVWMH, which

were extended rims or caps, and nonpathological PVWMH, which were pencil-thin rims or caps.

Classification of WMHs

Nonparametric methods such as kNN do not rely on predefined distributions, but on the actual distribution of the training samples [Clarke et al., 1993; Duda et al., 2001]. kNN has given superior results both in accuracy and reproducibility compared to some parametric methods [Clarke et al., 1993] in brain tissue classification, and its application in classifying WMH in multiple sclerosis has also achieved good results [Anbeek et al., 2004; Wu et al., 2006].

In general, kNN classification rule consists of a training procedure and a testing procedure. Training procedure is to use a small portion of the dataset to construct a classifier and then the testing procedure uses the classifier thus built to perform the classification task. These training samples are given in a multi-dimensional feature space and have labels associated with them, thus designating their class membership. In the testing procedure, unlabeled data points are classified by assigning it the label most frequently represented among the k nearest samples. A decision is made about a testing sample by examining the labels on the k nearest neighbors from the training samples and taking a vote [Duda et al., 2001]. In our implementation of kNN WMH classification, a label of WMH membership was assigned to each candidate WMH cluster after visual inspection of the initial WMH maps by a biomedical engineer (WW) in consultation with a neuropsychiatrist (PS) for training dataset setup.

Different from the previous tissue classification applications using kNN [Anbeek et al., 2004; Wu et al., 2006], this study used the cluster information of the candidate WMH rather than the individual voxel. The feature space defined in this study falls into four categories: (i) cluster intensity information; (ii) cluster spatial information; (iii) the intensity information of the voxels that surrounded the candidate WMH cluster; (iv) and cluster size in number of voxels (see Fig. 1).

For the first category of cluster intensities, once a candidate WMH cluster was identified, four measures were then incorporated in the cluster intensity information, i.e. the ratio of cluster mean over total brain tissue mean, and the ratio of cluster standard deviation over standard deviation of whole brain tissue for T1-weighted scan. Two equivalent ratios for FLAIR scan were also defined for this intensity category of feature space. The inclusion of WMH cluster intensity information from both FLAIR and T1-weighted scans was based on the fact that WMH appeared to be hyperintense in a FLAIR and hypointense in a T1-weighted scan comparing with normal white matter. The distance of the WMH centroid to the nearest edge of lateral ventricles was used as the cluster spatial information in the second category. The third group of features included the intensity information of the voxels, which form a "shell" around a candidate WMH cluster, i.e. the voxels that were connected with the candidate WMH cluster. To extract these surrounding voxels, we applied morphological dilation with a uniform 3D structure of 3 on each candidate WMH cluster, and mapped the 3D "shell" created by the dilation into the T1-weighted image of the subject. The mean and standard deviation of the "shell" voxels of the T1-weighted image were then calculated. The last category of the feature space was the cluster size of the number of voxels. The final dimension of the feature space was eight, including four features describing the cluster intensity, two characterizing the voxel property bordering the cluster, and one each for the candidate cluster spatial location in relation to the ventricles and the cluster size.

Accuracy of the kNN Classification

A candidate WMH cluster was categorized into one of four groups, i.e. DWMH (pathological), pathological PVWMH (pPVWMH) which were extended rims or caps in both size and intensity, non-pathological (pencil-thin and relatively not-so-bright) rims or caps (nPVWMH) and false WMH. In this study, only the WMH clusters that were considered as pathological, i.e. DWMH and pPVWMH were included in the WMH map (Figs. 1 and 2). The rationale for separating PVWMH into non-pathological and pathological rim/cap types of WMHs was that pencil-thin rims and caps have been considered normal anatomical variants by some studies [Enzinger et al., 2006; Fazekas et al., 1993]. Furthermore, partial-voluming of soft tissue and CSF around ventricles may produce hyperintense voxels similar to the WMHs. However, there also exist "large or extended" and very bright rims and caps that should be considered as pathological. The hyperintense periventricular areas were therefore classified as nPVWMH (considered as normal in this study) or pPVWMH (considered as pathological) which were both highly hyperintensive and spatially extensive. In our final analysis of WMHs, DWMH and pPVWMH (extended rims and caps) were considered as WMH while nPVWMH (pencil-thin-line type of periventricular voxel clusters) were also extracted but not classified as WMHs in this study. Nevertheless, they will be included in further analyses to find out if they play any role in the progression of WMHs. Some of the kNN classification results are shown in Figure 2.

To predict the performance of this implementation of kNN rule, we assessed its error rate on a data set that was not part of the formation of the classifier. Both the aim of this procedure and the way it was carried out were different from the visual rating of the WMHs as described in a separate section. The aim of this procedure was to build up a kNN classifier and check the performance of the method while the visual rating was to correlate our method with an accepted visual scale. To do this, we randomly selected 20 clusters for each of these four classes from the testing samples containing candidate WMH clusters. As true WMHs are sporadic, and DWMH are uncom-

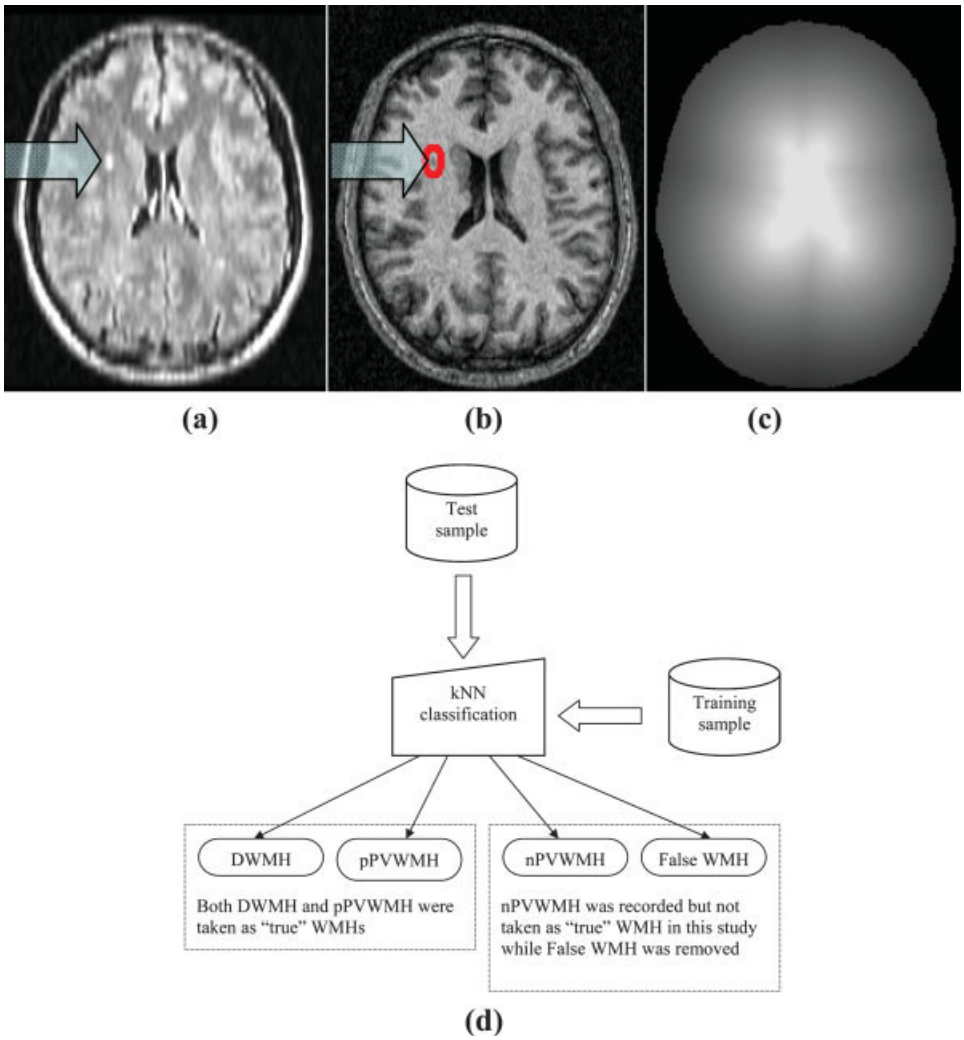

Figure 1.

Preparation for kNN classification feature space: (**a**) A candidate WMH cluster is extracted from FLAIR image. The ratio of the mean intensity of this candidate WMH cluster over the intensity of brain tissue is then calculated. (**b**) The voxels that surround this candidate WMH cluster form a 3D "shell" around the cluster, and from the co-registered T1-weighted image the "shell" is extracted and its intensity information is calculated. WMH cluster size (number of voxels in the cluster) is also calculated. (**c**) The spatial information of this candidate WMH cluster with respect to the nearest edge of the lateral ventricles is obtained from this "ventricle distance map". The voxel intensity of this ventricle distance map is the distance of that voxel to the nearest edge of the lateral ventricles. (**d**) Flowchart of kNN classification implementation. [Color figure can be viewed in the online issue, which is available at www.interscience.wiley.com.]

mon in this age group, in order to collect 20 DWMH clusters, we randomly inspected 26 images. The candidate WMH clusters in each of these images were classified visually by simultaneously viewing both FLAIR and T1-weighed images. The comparison between the automated kNN classification and visual classification showed that a 92.5% accuracy for separating pathological WMH (including DWMH and pPVWMH) from false WMH clusters was achieved when $k = 3$ was used. The accuracy rate for separating pPVWMH and nPVWMH was 85%, while DWMH was classified 100% correctly using $k = 3$.

We have designed and implemented our algorithms with Matlab® programming language and script language PERL, and the kNN classification of the candidate WMH clusters was carried out using Weka software package [Witten and Frank, 2005], version 3.4.8.

Manual Removal of Large Infarcts

Large infarcts were visually detected in 3 of these 428 subjects and were removed manually before WMH detection and classification procedures.

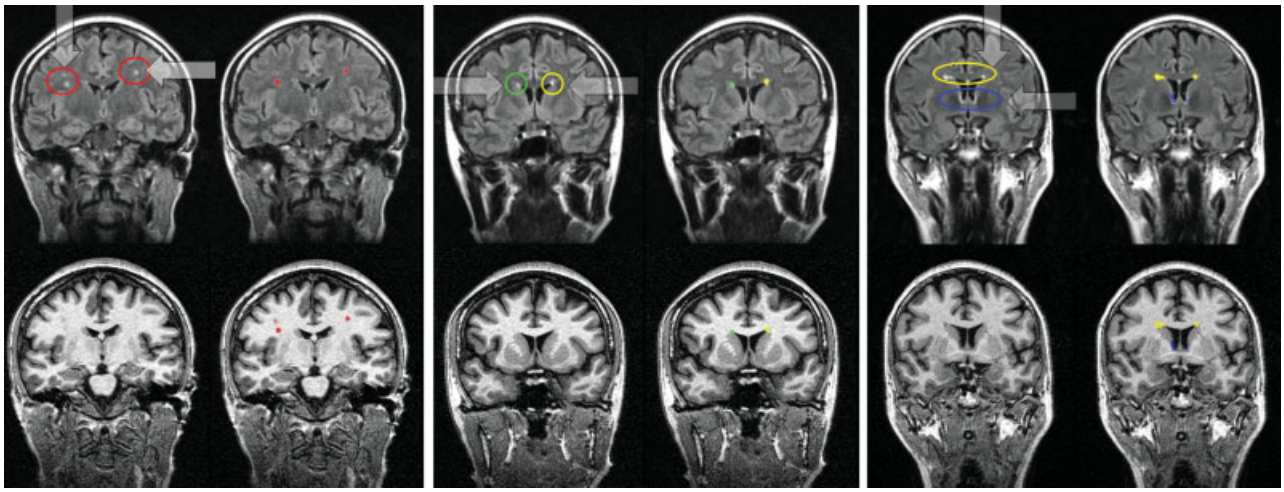

Figure 2.
Some kNN classification results. Red: deep white matter hyperintensity (DWMH) clusters; yellow: extended rims or caps that are pathological periventricular WMH (pPVWMH) and both DWMH and pPVWMH are counted as WMHs in the data analysis; green and blue: pencil-thin rims (blue) or caps (green), which are not considered as pathological WMHs and thus not included in the analysis). [Color figure can be viewed in the online issue, which is available at www.interscience.wiley.com.]

Visual Rating of WMHs

To compare and correlate our automated method with widely used visual rating methods, we visually rated the scans of 60 subjects. These 60 subjects were randomly selected and both their FLAIR and T1-weighted scans were used for the visual rating. Data were transferred to a DELL Precision 380 workstation running Windows XP® and analyzed using ANALYZE® (Biomedical Imaging Resource, Mayo Foundation.). T1-weighed scans were co-registered and then re-sliced onto the FLAIR scans of the same subject so that FLAIR and T1-weighted structural images could be placed side by side on the monitor simultaneously for visual rating. The scans were independently and blindly rated by a neurologist (XC) using the rating methods of Fazekas et al. [Fazekas et al., 1987] on a 0–3 scale for deep white matter (absence, punctate or foci, beginning of large or large, and confluent) and periventricular regions (absence, caps or pencil-thin lining, smooth "halo", and extending into deep white matter).

General Statistical Data Analysis

We observed that WMH volumes were strongly skewed towards the lower end (with total $n = 428$, skewness = 13.7; kurtosis = 231.3; with $n = 218$, including only those who had WMH, skewness = 10.2, kurtosis = 126.1). Natural logarithmic transform of WMH volumes was hence used in the analyses (with $n = 428$, skewness = 0.40; kurtosis = −1.41; with $n = 218$, skewness = −0.096; kurtosis = −0.38). SPSS (version 14; SPSS, Chicago, IL) was used for statistical data analysis.

RESULTS

Participants Without WMHs

210 (male 93, female 117) (49.1%) participants were free of WMHs if nPVWMH clusters were considered as normal anatomical variants. Of these, 43 (male 16, female 27) were totally free of any real or suspicions WMHs including pencil-thin caps or lines. There were no differences in age, sex, years of education and between the two groups that had or did not have WMHs as listed in Table II.

Participants With WMHs

Of the 218 (male 103, female 115) subjects with WMHs, 72 (16.8% of the total 428) had only periventricular WMH (extended rims and/or caps) and 92 (21.5%) only DWMH, and the remaining 54 (12.6%) subjects had both pPVWMH and DWMH. As expected, the total WMH volumes for the subjects who had both pPVWMH and DWMH were greater ($P < 0.001$) than those who had DWMH only, with the mean (SD) WMH for the two groups being 1,386.42 (2,822.53) mm^3, and 142.11 (238.08) mm^3 respectively. The average number and volume of DWMH detected in the former were calculated as 3.56 (3.55) and 338.47 (889.11) mm^3, both also greater ($P = 0.005$ for the number of DWMH occurrences, and $P = 0.047$ for the DWMH volumes) than those who had DWMH only, which were 2.30 (1.80) for the number of DWMH occurrences and 142.11 (238.08) mm^3, respectively. The mean (SD) WMH volume for those who had pPVWMH (only extended rims and/or caps considered) only was 435.27 (547.33) mm^3 and the

TABLE II. Comparisons of demographic characteristics and volumetric measures between subjects with and without white matter hyperintensities (WMHs)

Variables	WMHS		df	t/χ^2	*P* Value
	Yes (n = 218)	No (n = 210)			
Age (years)	46.77 (1.41)	46.61 (1.44)	426	1.100	0.272
Sex, male (%)	103 (47.25)	93 (44.29)	1	0.378	0.539
Education (years)	14.82 (2.18)	14.78 (2.37)	425	0.187	0.851
Right-handed (%)	196 (89.91)	185 (88.10)	1	0.360	0.549
Scanner A (%)	89 (40.83)	74 (35.24)	1	1.416	0.234
Total intracranial volume (TIV)	1.46 (0.14)	1.44 (0.13)	426	1.621	0.106
Gray matter volume (GM)	0.72 (0.07)	0.71 (0.07)	426	1.238	0.216
White matter volume (WM)	0.47 (0.06)	0.46 (0.05)	426	2.290	0.022*
Cerebrospinal fluid volume (CSF)	0.27 (0.06)	0.27 (0.06)	426	0.209	0.834

*P = 0.08 if controlling for TIV.

mean (SD) WMH volume for all those 218 subjects who had been detected with WMHs of one type or another was 547.15 (1,522.02) mm^3 or 0.547 (1.52) ml.

We found that the majority of DWMHs were punctate or focal in size. The mean (SD) number of DWMH occurrences (clusters) was 2.77 (2.65) in the 146 subjects who had DWMHs, and the mean (SD) volume for each DWMH cluster was 77.52 mm^3, which would form a sphere of about 5.29 mm diameter. WMHs in the deep white matter may appear as small punctate to large confluent lesions. We categorized these DWMH clusters according to their sizes. They were considered as punctate if their diameter was smaller than 3 mm, focal if diameter between 3 and 12 mm, or large if diameter greater than 12 mm. Of the total 411 DWMH clusters found in the 146 subjects, 206 (50.1%) were punctate with a mean diameter of 2.46 mm (1.85), 202 (49.1%) were focal with a mean diameter of 5.12 mm (5.77), and 3 (0.7%) large with a mean diameter 14.71 mm (11.51). 42 (28.7%) of these 146 subjects had punctate DWMH only, 39 (26.7%) focal only, 63 (43.2%) both punctate and focal, and only 2 (1.3%) had large DWMH.

Spatial Distribution of WMHs

As we used kNN rules to classify each WMH cluster into either DWMH or PVWMH (extended rims and caps), we were open to two methods of studying the distribution of WMH volumes in relation to the distance from the lateral ventricles, i.e. (a) using the kNN classification regardless of how far away the WMH extended itself from the ventricles into the subcortical area in case of large continuous WMH cluster; or (b) defining a ring of a predetermined width around the walls of the ventricles, with the WMHs within the ring then being classified as PVWMH, and those outside as DWMH [DeCarli et al., 2005b]. Figure 3b shows the histogram of DWMH volume in relation to the distance form the ventricular wall. The DWMH clusters shown in the figure were classified using kNN rules. Centrum semiovale was as likely to have WMH as the WM close to the cortex, i.e. there was no clear pattern emerging from this histogram about the anatomical distribution of the DWMH. On the other hand, the majority of WMHs were found to be close to the ventricles if the total volumes were considered (see Fig. 3a). When a 6 mm thick band of white matter adjacent to the lateral ventricles was defined, the total WMH volume located within this band was about 74.42% (n = 218; 407.18 mm^3) of the whole brain WMH volumes (547.16 mm^3). Figure 4 shows the anatomical distribution of WMHs in the 218 subjects who were observed to have WMHs. Table IV shows the WMH distribution in terms of lobar regions.

Sex Difference

Although both the mean volume and number of WMHs were greater for female subjects, the sex differences were not statistically significant (see Table III). It should be noted that the two subjects who had large (confluent) WMHs were both female.

There was no significant sex difference if we considered only those subjects who had WMHs. The mean whole brain WMH volumes for female subjects (n = 115) were 644.92 (2,013.10) mm^3, and male subjects 438.00 (613.38) mm^3 (P = 0.317). DWMH volumes as classified by kNN rule were 189.89 (642.63) mm^3 for female subjects (n = 81), and 92.37 (171.33) mm^3 (P = 0.161) for male subjects (n = 65), respectively.

Correlation of the Automated Method With a Visual Rating Method

As the automated method produced quantitative values in both WMH volume and the number of occurrences of WMHs (clusters), the correlations between the visual rating scores and automated method results were examined. The Pearson's correlation coefficient for the total visual rating score (sum of all the scores) and the number of WMH cluster occurrences of the whole brain (automated method)

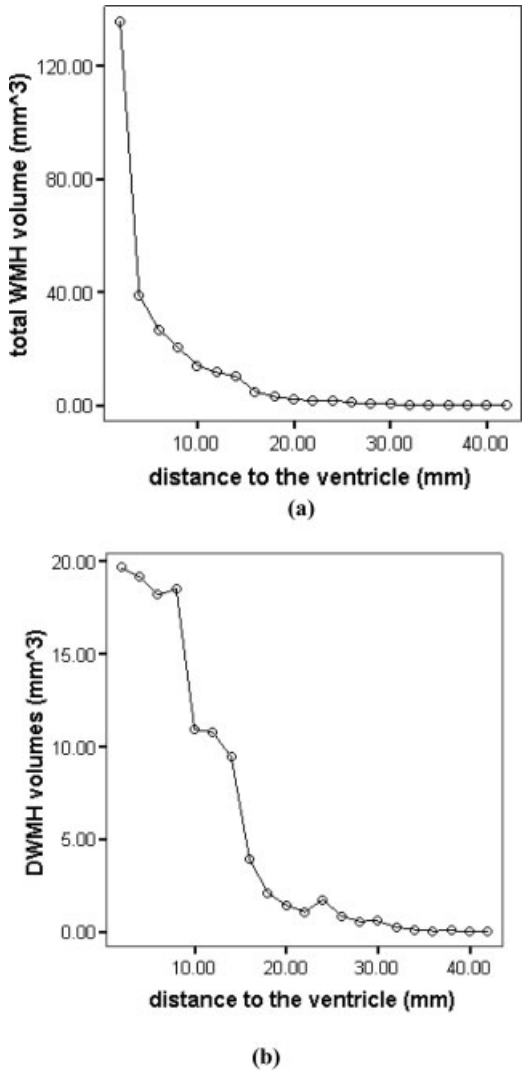

Figure 3.
The relationship between WMH volumes and the distance from the lateral ventricles, using (**a**) whole brain WMH volumes (mean) and (**b**) deep WMH volumes (mean). Note that these DWMH clusters were classified by kNN algorithm.

was $r = 0.692$ at significant level of $P < 0.001$. However, the correlation strength dropped to $r = 0.503$ ($P < 0.001$) between the total visual rating scores and WMH volumes generated by automated method. When examining deep white matter and periventricular regions separately, we found that WMHs in the deep white matter had stronger correlations. The correlations were $r = 0.823$ ($P < 0.001$) between DWMH visual ratings and the number of DWMH occurrences and $r = 0.697$ ($P < 0.001$) between DWMH visual ratings and DWMH volumes, respectively. On the other hand, the correlations were $r = 0.428$ ($P < 0.001$) between PVWMH visual ratings and the number of PVWMH occurrences and $r = 0.279$ ($p < 0.001$) between PVWMH visual ratings and PVWMH volumes, respectively.

DISCUSSION

Most WMH studies focus either on disease-specific groups, such as stroke [Bokura et al., 2006; Jokinen et al., 2005; Leaper et al., 2001; Schmidt et al., 2003, 2005; van den Heuvel et al., 2004; Wen and Sachdev, 2004b], drug abuse [Bae et al., 2006], Parkinson's disease [Beyer et al., 2006; Marshall et al., 2006], mild cognitive impairment (MCI) [DeCarli et al., 2001], impaired mobility [Guttmann et al., 2000], depression [Ehrlich et al., 2005; Iosifescu et al., 2006; Jorm et al., 2005; Lin et al., 2005; Thomas et al., 2003; van Straaten et al., 2006b], schizophrenia [Bagary et al., 2003; Sachdev and Brodaty, 1999] and other disorders [Altaf et al., 2006; Awad et al., 1986; Bleecker et al., in press; Gunstad et al., 2005; Murray et al., 2005; Ovbiagele and Saver, 2006; van Straaten et al., 2006a] or study the "healthy" elderly population [Leaper et al., 2001; Ylikoski et al., 1995; van den Heuvel, et al. and PROSPER Study Group, 2004]. Some previous studies [Enzinger et al., 2006; Wen and Sachdev, 2004b] have shown high prevalence of WMHs for the community residents over 60. However, there has been little information on the younger population about the prevalence and topography of WMHs. This study of the 44–48 age group sampled randomly from community residents is therefore unique in examining individuals considered to be at low risk of these lesions and possibly harboring them at their inception.

It is noteworthy that nearly one-half participants in this study were found to have WMHs. The majority of these were periventricular, but focal WMHs were common in the deep white matter areas. Not all the WMHs started from the periventricular area and then expanded into deep white matter forming large and confluent WMHs [Barkhof and Scheltens, 2006]. There were no significant differences in WMH volumes and distribution between men and women in this age group.

An important finding of our study is the high prevalence of WMHs in asymptomatic individuals below the age of 50, with nearly one in two individuals so affected. Our study has two advantages over previous work: (a) we had a large sample in a small age range, and (b) we designed an algorithm for the accurate detection and classification of early WMH clusters which are generally very small in size, i.e. punctate or focal WMHs, and which could easily be missed if using visual ratings or some other automated methods [Wen and Sachdev, 2004b]. The prevalence of 50.9% if DWMH and extended rims and caps were included, and 34.11% if only DWMH were considered, found in this study reflects the high sensitivity of the method. We wish to emphasize that all WMH clusters that were automatically detected using the algorithm were

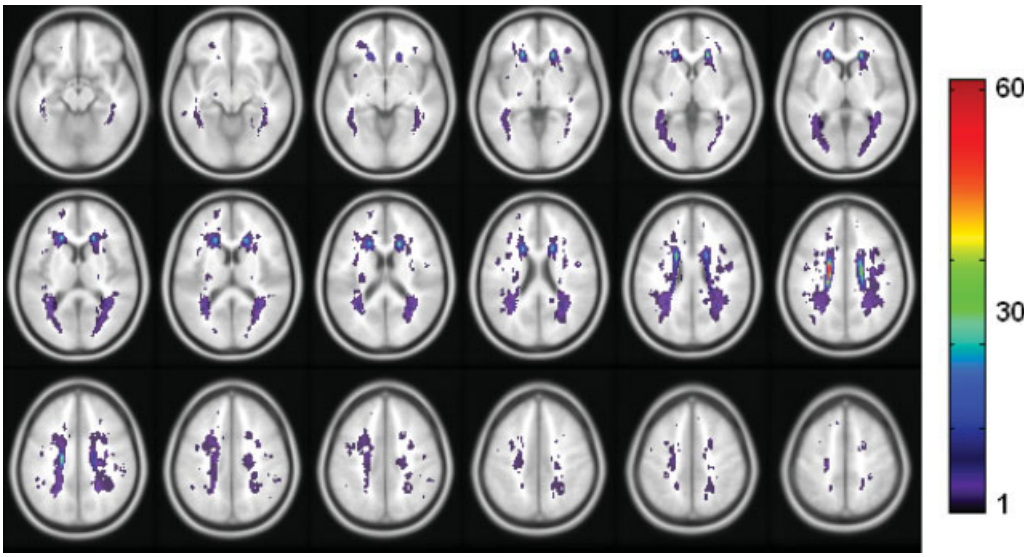

Figure 4.

Spatial distribution of WMHs. Map of the sample (n = 218) with WMHs in the standard space. The WMHs were mapped into the standard space from their each individual acquisition space. The color bar denotes the number of WMH occurrences of the anatomical location. [Color figure can be viewed in the online issue, which is available at www.interscience.wiley.com.]

subsequently examined visually, attesting to the validity of the method.

The pathological significance of WMHs that are strictly peri-ventricular, comprising pencil-thin rims and caps, has been questioned, and they have been often regarded as normal variants [Enzinger et al., 2006; Fazekas et al., 2006]. Considering this, if we exclude all the PVWMH even the extended rims and caps from prevalence figures, the prevalence of DWMH of 34.11% should still be regarded as high. The majority of the DWMH in our study participants were either punctate or focal, suggesting that these DWMH were possibly at an early stage of their development. One must conclude that at some time in mid-life, WMHs begin to make their appearance in the brains of healthy individuals. MRI-postmortem histopathologic studies suggest that punctate DWMH are not associated with infarction, but represent areas of reduced myelination and atrophy of the neuropil around fibrohyalinotic arterioles as well as perivenous damage [Fazekas et al., 1993]. They therefore possibly reflect small vessel disease whose manifestations appear much earlier in life than has generally been believed. The lack of pathological verification of these lesions makes it a tentative conclusion.

TABLE III. Comparisons of male and female in relation to WMH volumes and occurrences

	Total (N = 428)	Male (N = 196)	Female (N = 232)	Comparisons between male and female	
				df	P
Whole brain WMH volume (mm^3) mean and (SD)	278.69 (1119.04)	230.17 (494.85)	319.68 (1450.65)	426	0.577
DWMH[a] volume	73.25 (351.65)	48.54 (132.26)	94.13 (461.37)	426	0.182
pPVWMH[a] (extended rims and caps) volume	205.44 (1052.12)	181.63 (471.48)	225.56 (1362.95)	426	0.513
WMH volumes within 6 mm of peri-ventricular ring	207.4 (785.92)	192.98 (462.46)	219.57 (980.25)	426	0.656
WMH volumes outside 6 mm of peri-ventricular ring	71.29 (374.62)	37.19 (101.26)	100.11 (498.94)	426	0.083
Number of DWMH[a] clusters	0.94 (2.03)	0.84 (1.71)	1.03 (2.26)	426	0.315
Number of pPVWMH[a] clusters	0.43 (0.76)	0.44 (0.75)	0.42 (0.77)	426	0.780

[a] These values were calculated over the whole sample population of 428 subjects, regardless of whether the subject had WMH or not.

TABLE IV. The mean (SD) volumes of WMH (mm^3) were computed from 428 (m/f = 196/232) subjects' FLAIR sequence MR scans and are listed for each brain region

	Frontal Mean (SD)	Temporal Mean (SD)	Parietal Mean (SD)	Occipital Mean (SD)	Cerebrum Mean (SD)	Brain Stem Mean (SD)	Whole Brain Mean (SD)
All subjects n = 428	101.19 (348.98)	6.40 (83.60)	163.34 (714.28)	7.70 (82.77)	0.00 (0.00)	0.035 (0.725)	278.79 (1119.04)
Men n = 196	101.72 (308.98)	2.19 (18.40)	123.32 (253.37)	2.81 (21.63)	0.00 (0.00)	0.077 (1.07)	230.17 (494.85)
Women n = 232	100.74 (380.18)	9.95 (112.27)	197.15 (941.48)	11.83 (110.59)	0.00 (0.00)	0.00 (0.00)	319.68 (1450.65)

The partition of the lobes and other brain regions was described by Wen and Sachdev, 2004b (Fig. 2a). None of the comparisons on the lobar WMH volumes between men and women was significant.

Some authors [DeCarli et al., 2005a] have not supported the subcategorization of WMHs into periventricular and deep WMHs, arguing that when WMHs progress, they become confluent and eventually contiguous with the ventricles. However, we have previously suggested that the pathophysiology and functional significance of PVMH may be somewhat different from DWMH [Sachdev and Wen, 2005]. MRI-histopathological studies have revealed that periventricular WMHs such as rims, caps and rims directly adjacent to the ventricles of high T2 signal reflect relatively mild pathology [Fazekas et al., 1993; Takao et al., 1999], and are sometimes considered as normal anatomical variants. On the other hand, DWMH are shown to be associated with pathology varying from myelin pallor as in punctate and focal patches [Takao et al., 1999] to ischemic tissue damage as in large and confluent DWMHs [Fazekas et al., 1993]. Our approach, using a boundary delineation in the periventricular region, makes it possible to examine the significance of WMH as a single group or two subgroups, thereby elaborating on this debate. When we examined the extent of WMHs as a function of the distance from the ventricular wall, we found a distribution that was not consistent with the exclusive spread of WMHs from the periventricular region outward into the deep white matter (see Fig. 4).

One of the strengths of this study is that the sample comprised a large community-based asymptomatic cohort and our analysis suggested that the sample was reasonably representative. The narrow age range permitted topographic characterization of WMHs at an interesting period in life. Of course, the age range limits the generalizability of the findings to other age groups. However, we considered this to be an informative age group, being perimenopausal in women, and being at the age at which clinical manifestations of vascular disease are still uncommon. A further limitation of the study is that we partitioned the brain into lobar regions of interest (ROIs) and described the WMH volumes and occurrence in these. A better WMH localization strategy would possibly use the information on white matter tracts, but this must await the availability of a detailed electronic version of a white matter atlas.

We have also examined the correlations between the quantitative results generated by the automated method and the visual rating scores. Overall, automated method demonstrated good correlations with the visual ratings, either separately in deep white matter, periventricular regions or in whole brain measures, with the highest correlations in DWMH occurrences ($r = 0.823$, $P < 0.001$).

In conclusion, this study suggests that WMHs are common in community-dwelling healthy subjects in their 40s, although the burden of these lesions is small in terms of their volumes. The majority of these lesions are in the periventricular region, but the data suggest that lesions in the deep white matter are not necessarily an extension of periventricular lesions and may arise independently. Whether WMHs have an impact on the functioning of individuals in their 40s remains to be examined.

ACKNOWLEDGMENTS

The PATH project involved many researchers, in particular Helen Christensen, Anthony Jorm, Bryan Rodgers (Chief Investigators), Trish Jacomb, Karen Maxwell, June Cullen, and a team of interviewers.

REFERENCES

Altaf N, Daniels L, Morgan PS, Lowe J, Gladman J, MacSweeney ST, Moody A, Auer DP (2006): Cerebral white matter hyperintense lesions are associated with unstable carotid plaques. Eur J Vasc Endovasc Surg 31:8–13.

Anbeek P, Vincken KL, van Osch MJP, Bisschops RHC, van der Grond J (2004): Automatic segmentation of different-sized white matter lesions by voxel probability estimation. Med Image Anal 8:205–215.

Ashburner J, Friston K (1997): Multimodal image coregistration and partitioning--A unified framework. NeuroImage 6:209–217.

Ashburner J, Friston KJ (1999): Nonlinear spatial normalization using basis functions. Hum Brain Mapping 7:254–266.

Ashburner J, Friston KJ (2005): Unified segmentation. NeuroImage 26:839–851.

Awad IA, Spetzler RF, Hodak JA, Awad CA, Carey R (1986): Incidental subcortical lesions identified on magnetic resonance imaging in the elderly. I. Correlation with age and cerebrovascular risk factors. Stroke J Cereb Circulation 17:1084–1089.

Bae SC, Lyoo IK, Sung YH, Yoo J, Chung A, Yoon SJ, Kim DJ, Hwang J, Kim SJ, Renshaw PF (2006): Increased white matter hyperintensities in male methamphetamine abusers. Drug Alcohol Dependence 81:83–88.

Bagary MS, Symms MR, Barker GJ, Mutsatsa SH, Joyce EM, Ron MA (2003): Gray and white matter brain abnormalities in first-

episode schizophrenia inferred from magnetization transfer imaging. Arch Gen Psychiatry 60:779–788.
Barkhof F, Scheltens P (2006): Is the whole brain periventricular? J Neurol Neurosurg Psychiatry 77:143–144.
Beyer MK, Aarsland D, Greve OJ, Larsen JP (2006): Visual rating of white matter hyperintensities in Parkinson's disease. Movement Disorders 21:223–229.
Bleecker ML, Ford DP, Vaughan CG, Walsh KS, Lindgren KN (2007): The association of lead exposure and motor performance mediated by cerebral white matter change. NeuroToxicology 28:318–323.
Bokura H, Kobayashi S, Yamaguchi S, Iijima K, Nagai A, Toyoda G, Oguro H, Takahashi K (2006): Silent brain infarction and subcortical white matter lesions increase the risk of stroke and mortality: A prospective cohort study. J Stroke Cerebrovascular Dis 15:57–63.
Clarke LP, Velthuizen RP, Phuphanich S, Schellenberg JD, Arrington JA, Silbiger M (1993): MRI: Stability of three supervised segmentation techniques. Magn Reson Imaging 11:95–106.
de Leeuw FE, de Groot JC, Achten E, other authors (2001): Prevalence of cerebral white matter lesions in elderly people: A population based magnetic resonance imaging study. The Rotterdam Scan Study. J Neurol Neurosurg Psychiatry 70:9–14.
DeCarli C, Miller BL, Swan GE, Reed T, Wolf PA, Carmelli D (2001): Cerebrovascular and brain morphologic correlates of mild cognitive impairment in the National Heart, Lung, and Blood Institute Twin Study. Arch Neurol 58:643–647.
DeCarli C, Fletcher E, Ramey V, Harvey D, Jagust WJ (2005a): Anatomical mapping of white matter hyperintensities (WMH): Exploring the relationships between periventricular WMH, deep WMH, and total WMH burden. [see comment]. Stroke 36:50–55.
DeCarli C, Fletcher E, Ramey V, Harvey D, Jagust WJ (2005b): Anatomical mapping of white matter hyperintensities (WMH): Exploring the relationships between periventricular WMH, deep WMH, and total WMH burden. Stroke J Cereb Circ 36: 50–55.
Duda RO, Hart PE, Stork DG (2001): Pattern Classification, 2nd ed. New York, John Wiley & Sons.
Ehrlich S, Breeze JL, Hesdorffer DC, Noam GG, Hong X, Alban RL, Davis SE, Renshaw PF (2005): White matter hyperintensities and their association with suicidality in depressed young adults. J Affective Disord 86:281–287.
Enzinger C, Smith S, Fazekas F, Drevin G, Ropele S, Nichols T, Behrens T, Schmidt R, Matthews PM (2006): Lesion probability maps of white matter hyperintensities in elderly individuals: Results of the Austrian stroke prevention study. J Neurol 253: 1064–1070.
Fazekas F (1989): Magnetic resonance signal abnormalities in asymptomatic individuals: Their incidence and functional correlates. Eur Neurol 29:164–168.
Fazekas F, Chawluk JB, Alavi A, Hurtig HI, Zimmerman RA (1987): MR signal abnormalities at 1.5 T in Alzheimer's dementia and normal aging. Am J Roentgenol 149:351–356.
Fazekas F, Kleinert R, Offenbacher H, Schmidt R, Kleinert G, Payer F, Radner H, Lechner H (1993): Pathologic correlates of incidental MRI white matter signal hyperintensities. Neurology 43:1683–1689.
Gunstad J, Cohen RA, Tate DF, Paul RH, Poppas A, Hoth K, Macgregor KL, Jefferson AL (2005): Blood pressure variability and white matter hyperintensities in older adults with cardiovascular disease. Blood Pressure 14:353–358.
Guttmann CR, Benson R, Warfield SK, Wei X, Anderson MC, Hall CB, bu-Hasaballah K, Mugler JP III, Wolfson et al. (2000): White matter abnormalities in mobility-impaired older persons. Neurology 54:1277–1283.
Helenius J, Soinne L, Salonen O, Kaste M, Tatlisumak T (2002): Leukoaraiosis, ischemic stroke, and normal white matter on diffusion-weighted MRI. Stroke J Cereb Circ 33:45–50.
Hopkins RO, Beck CJ, Burnett DL, Weaver LK, Victoroff J, Bigler ED (2006): Prevalence of white matter hyperintensities in a young healthy population. J Neuroimaging 16: 243–251.
Iosifescu DV, Renshaw PF, Lyoo IK, Lee HK, Perlis RH, Papakostas GI, Nierenberg AA, Fava M (2006): Brain white-matter hyperintensities and treatment outcome in major depressive disorder. Br J Psychiatry J Mental Sci 188:180–185.
Jokinen H, Kalska H, Mantyla R, Ylikoski R, Hietanen M, Pohjasvaara T, Kaste M, Erkinjuntti T (2005): White matter hyperintensities as a predictor of neuropsychological deficits post-stroke. [see comment]. J Neurol Neurosurg Psychiatry 76:1229–1233.
Jorm AF, Anstey KJ, Christensen H, de Plater G, Kumar R, Wen W, Sachdev P (2005): MRI hyperintensities and depressive symptoms in a community sample of individuals 60–64 years old. Am J Psychiatry 162:699–705.
Le Bihan D (1991): Molecular diffusion nuclear magnetic resonance imaging. Magn Reson Quart 7:1–30.
Leaper SA, Murray AD, Lemmon HA, Staff RT, Deary IJ, Crawford JR, Whalley LJ (2001): Neuropsychologic correlates of brain white matter lesions depicted on MR images: 1921 Aberdeen Birth Cohort. Radiology 221:51–55.
Lin HF, Kuo YT, Chiang IC, Chen HM, Chen CS (2005): Structural abnormality on brain magnetic resonance imaging in late-onset major depressive disorder. Kaohsiung J Med Sci 21:405–411.
Longstreth WT Jr, Manolio TA, Arnold A, Burke GL, Bryan N, Jungreis CA, Enright PL, O'Leary D, Fried et al. (1996): Clinical correlates of white matter findings on cranial magnetic resonance imaging of 3301 elderly people. The Cardiovascular Health Study. Stroke J Cereb Circ 27:1274–1282.
Marshall GA, Shchelchkov E, Kaufer DI, Ivanco LS, Bohnen NI (2006): White matter hyperintensities and cortical acetylcholinesterase activity in parkinsonian dementia. Acta Neurologica Scandinavica 113:87–91.
Mascalchi M, Moretti M, la Nave R, other authors (2002a): Longitudinal evaluation of leukoaraiosis with whole brain ADC histograms. Neurology 59:938–940.
Mascalchi M, Tessa C, Moretti M, la Nave R, Boddi V, Martini S, Inzitari D, Villari N (2002b): Whole brain apparent diffusion coefficient histogram: A new tool for evaluation of leukoaraiosis. J Magn Reson Imaging 15:144–148.
Murray AD, Staff RT, Shenkin SD, Deary IJ, Starr JM, Whalley LJ (2005): Brain white matter hyperintensities: Relative importance of vascular risk factors in nondemented elderly people. Radiology 237:251–257.
Oldfield RC (1971): The assessment and analysis of handedness: the Edinburgh inventory. Neuropsychologia 9:93–113.
Ovbiagele B, Saver JL (2006): Cerebral white matter hyperintensities on MRI: Current concepts and therapeutic implications. [Review] [72 refs]. Cerebrovascular Diseases 22:83–90.
Rovaris M, Filippi M, Calori G, Rodegher M, Campi A, Colombo B, Comi G (1997): Intra-observer reproducibility in measuring new putative MR markers of demyelination and axonal loss in multiple sclerosis: A comparison with conventional T2-weighted images. J Neurol 244:266–270.

Sachdev P, Brodaty H (1999): Quantitative study of signal hyperintensities on T2-weighted magnetic resonance imaging in late-onset schizophrenia. Am J Psychiatry 156:1958–1967.

Sachdev P, Wen W (2005): Should we distinguish between periventricular and deep white matter hyperintensities? Stroke 36:2342–2343.

Scheltens P, Barkhof F, Leys D, Wolters EC, Ravid R, Kamphorst W (1995): Histopathologic correlates of white matter changes on MRI in Alzheimer's disease and normal aging. Neurology 45:883–888.

Schmidt R, Fazekas F, Reinhart B, Kapeller P, Fazekas G, Offenbacher H, Eber B, Schumacher M, Freidl W (1996): Estrogen replacement therapy in older women: A neuropsychological and brain MRI study. J Am Geriatrics Soc 44:1307–1313.

Schmidt R, Schmidt H, Kapeller P, Lechner A, Fazekas F (2002): Evolution of white matter lesions. Cerebrovasc Dis (Basel, Switzerland) 13:16–20.

Schmidt R, Enzinger C, Ropele S, Schmidt H, Fazekas F (2003): Progression of cerebral white matter lesions: 6-year results of the Austrian Stroke Prevention Study. Lancet 361:2046–2048.

Schmidt R, Ropele S, Enzinger C, Petrovic K, Smith S, Schmidt H, Matthews PM, Fazekas F (2005): White matter lesion progression, brain atrophy, and cognitive decline: The Austrian Stroke Prevention Study. Ann Neurol 58:610–616.

Smith CD, Snowdon D, Markesbery WR (2000): Periventricular white matter hyperintensities on MRI: Correlation with neuropathologic findings. J Neuroimaging: Official J Am Soc Neuroimaging 10:13–16.

Takao M, Koto A, Tanahashi N, Fukuuchi Y, Takagi M, Morinaga S (1999): Pathologic findings of silent hyperintense white matter lesions on MRI. J Neurol Sci 167:127–131.

Thomas AJ, O'Brien JT, Barber R, McMeekin W, Perry R (2003): A neuropathological study of periventricular white matter hyperintensities in major depression. J Affective Disorders 76:49–54.

van den Heuvel DM, dmiraal-Behloul F, ten DV, other authors (2004): Different progression rates for deep white matter hyperintensities in elderly men and women. Neurology 63:1699–1701.

van den Heuvel DMJ, ten Dam VH, de Craen AJM, other authors (2006): Increase in periventricular white matter hyperintensities parallels decline in mental processing speed in a non-demented elderly population. J Neurol Neurosurg Psychiatry 77:149–153.

van Straaten EC, Fazekas F, Rostrup E, other authors (2006a): Impact of white matter hyperintensities scoring method on correlations with clinical data: The LADIS study. Stroke 37:836–840.

van Straaten ECW, Fazekas F, Rostrup E, other authors (2006b): Impact of white matter hyperintensities scoring method on correlations with clinical data: The LADIS Study. Stroke J Cereb Circ 37:836–840.

Wells I II, Viola P, Atsumi H, Nakajima S, Kikinis R (1996): Multimodal volume registration by maximization of mutual information. Med Image Anal 1:35–51.

Wen W, Sachdev P (2004a): The topography of white matter hyperintensities on brain MRI in healthy 60- to 64-year-old individuals. NeuroImage 22:144–154.

Wen W, Sachdev PS (2004b): Extent and distribution of white matter hyperintensities in stroke patients: The Sydney Stroke Study. Stroke 35:2813–2819.

Witten IH, Frank E (2005): Data Mining: Practical Machine Learning Tools and Techniques, 2nd ed. San Francisco, Elsevier.

Wu Y, Warfield SK, Tan IL, Wells WM III, Meier DS, van Schijndel RA, Barkhof F, Guttmann CRG (2006): Automated segmentation of multiple sclerosis lesion subtypes with multichannel MRI. NeuroImage 32:1205–1215.

Ylikoski A, Erkinjuntti T, Raininko R, Sarna S, Sulkava R, Tilvis R (1995): White matter hyperintensities on MRI in the neurologically nondiseased elderly. Analysis of cohorts of consecutive subjects aged 55 to 85 years living at home. Stroke J Cereb Circ 26:1171–1177.

Ylikoski R, Ylikoski A, Erkinjuntti T, Sulkava R, Raininko R, Tilvis R (1993): White matter changes in healthy elderly persons correlate with attention and speed of mental processing. Arch Neurol 50:818–824.